SSRG International Journal of Electronics and Communication Engineering
ISSN: 2348-8549/ https://doi.org/10.14445/23488549/IJECE-V13I6P117

Volume 13 Issue 6, 207-217, June 2026

Original Article

Low-Complexity Scalable Image Coding with Integrated Encryption Using Layered Block Truncation Code

Prabakaran MP[1], Ravindiran Asaithambi[2], Maria Jesi P[3], Jeya Bright Pankiraj[4]

[1]*Department of ECE, A.K.T Memorial College of Engineering and Technology, Kallakurichi, Tamil Nadu, India.*
2 Department of ECE, Sri Ramachandra Institute of Higher Education and Research, Tamilnadu, India.
3Department of CSE, Loyola Institute of Technology & Science, Thovalai, Tamilnadu, India.
4Department of ECE, Loyola Institute of Technology & Science, Thovalai, Tamilnadu, India.

[1]*Corresponding Author : drmpteaching@gmail.com*

Received: 19 March 2026 Revised: 18 April 2026 Accepted: 17 May 2026 Published: 27 June 2026

Abstract *- Even though some researchers have performed Scalable Coding on Encrypted (SCE) images using Block Truncation Code (BTC), its base layer reconstruction quality is poor with low Peak Signal to Noise Ratio (PSNR). There is still space to utilize residual quantization strategies to optimize the enhancement layer and achieve higher PSNR without increasing bitrate. This paper presents SCE Images using Layered BTC (LBTC). The pseudorandom number (PRND) operation and XOR operation are performed on the input grey image, and then the BTC technique is applied on the encrypted Image to get the base image. Then the base image is first quantized and then subtracted from the encrypted Image to get the enhancement image. Both the Base image and the enhancement image are dispatched. The enhancement image is added with the base image at the recipient side and then decrypted by using the XOR operation and PRND to get the rebuilt full original Image. The base image is rebuilt using the BTC technique and then decrypted by using the XOR operation and PRND to get the rebuilt base original Image. The proposed LBTC technique gives a higher PSNR of 41.73 dB than existing techniques, which reflects that the rebuilt full original Image has superior image quality*.

Keywords - *Image decryption, Image encryption, Image reconstruction, Layered BTC, Secured signal processing.*

1. Introduction

In the fast-paced world, there is a requirement for data size reduction and computational complexity, protection of data and privacy, which makes SCE necessary for the signal and information processing society. Few researchers had worked on SCE, but the rebuilt Image has lower PSNR, and still, there is ample space to improve the output image and performance metrics such as PSNR. The challenges, like data privacy and security in the area of Secure Signal Processing (SSP), are addressed by this method [1] and this method [2], which use the discrete Fourier transform to address this. The resource utilization is optimized by method [3] by use of adaptive filtering, and a composite signal is used in method [4] to address the challenges faced in SSP. The cloud-based buyer-seller watermarking protocol [5] is used to protect data in transactions. The effectiveness of hash fingerprinting techniques is presented in [6] to improve cybersecurity measures

In today's world, owing to the rise in the utilization of image data, there is a demand for reduced storage space and reduced bandwidth to lower the transmission cost. In order to meet this, it is first tried by first encrypting and then compressing by method [7] without compromising security. Similarly, in method [8], the encrypted data is compressed, which is unaware of the encryption key. The method [9] is proposed to reduce the size of the file by performing compression on the encrypted signal without compromising security. The problems faced in SSP have been tried to resolve by using the compressive sensing method [10] on encrypted images. The iterative reconstruction method discussed in [11] is carried out on encrypted images and has reconstructed the original Image at a reasonable level.

The process of applying scalability to signals will significantly improve PSNR, rebuild image quality, and reduce bit rate. Initially, scalability is carried on unencrypted signals. The reversible integer wavelet transform for scalable image coding is presented in [12], which achieved efficient image compression without compromising image quality. The EBCOT algorithm is discussed in [13], which achieved superior performance and scalability.

The SCE is first performed on [14], where a PRND is used for image encryption, the Hadamard transform is used for compressing encrypted data, scaled by a factor of 2, and at the

end, the primary Image is rebuilt using the Bilinear Interpolation Technique (BIT). The BTC technique has the advantage of lower computational complexity and lower storage requirement, and so the BTC technique can be used as an image compression in the process of SCE Images. The BTC technique used in [15] employs the mean as a doorstep value for two-level quantizers to build the binary block, and the primary Image is rebuilt with the variance and mean value of each non-overlapping block (NOL). The updation of BTC, namely Absolute Moment BTC (AMBTC) [16], uses the Max-level value and Min-level value to rebuild the primary Image. The SCE images are presented [17], where the input grey image is first encrypted using a PRND and then compressed using BTC and dispatched. At the recipient, the dispatched Image is first decrypted using a PRND, rebuilt using BTC Quantizers, and then scaled by a scaling factor of 2, and finally, the primary Image is rebuilt using the BIT.

The paper [18] presents a Reversible Data Hiding AMBTC (RDH-AMBTC) method where the Hamming code is used to embed secret data. A novel method, namely LBTC, which is superior to AMBTC and BTC in terms of Compression Ratio (CR), Weighted Peak Signal to Noise Ratio (wPSNR), Mean Squared Error (MSE), Bit Rate (BR), PSNR, Weighted Mean Squared Error (wMSE), computational time, and memory size. The novelty of the LBTC method over the existing SCE method is splitting the base layer and enhancement layer by using the residual quantization technique, which is optimized to rebuild the output image equivalent to the principal content with an improved PSNR value.

2. Related Works

2.1. Scalability using Hadamard Transform

In this approach [14], the input grey image is encrypted first by a PRND, and then it is split into gross details and refined details. The refined details are processed by the Hadamard transform, and both gross details and refined details are transmitted. The PRND acts as a private key and is released to the receiver. At the recipient, the refined details are decrypted by utilizing the private key, rounding and quantization are applied, a bilinear transform is applied, and then the refined details are processed by the Hadamard Transform. Finally, both gross details and refined details are merged to recreate the primary Image. However, the rebuilt Image exhibits a lower value than BTC, RDH-AMBTC, and the proposed LBTC in relation to CR, computing time, memory size, PSNR, MSE, wPSNR, wMSE, and BR.

2.2. Scalability using BTC

In this method [17], the primary Image is dissected into NOL of size 4×4, and then encrypted using a PRND. The PRND acts as a private key and is released in the middle of the dispatcher and the recipient. The encrypted Image is then compressed using the BTC technique using the two-level quantizers, which act as a doorstep value to obtain the binary pixel value, and then dispatched. The PRND operation is performed on the recipient to get the binary pixel value. Then the BTC technique, namely two-level quantizers, is applied to the binary pixel value of each NOL, and then dilated by a factor of 2, and finally the primary Image is rebuilt by utilizing the BIT.

However, the rebuilt Image exposes a lower value than RDH-AMBTC and the proposed LBTC but better than Hadamard Transform in relation to CR, computing time, memory size, PSNR, MSE, wPSNR, wMSE, and BR.

3. Proposed Method

The Schematic diagram of LBTC is displayed in Figure 1. The primary Image is encrypted by utilizing a PRND and an XOR operation. Then the base layer is procured by performing the BTC technique on the encrypted Image, and the output acts as a base image. The enhancement image is obtained by quantizing the base image, and then the encrypted output is subtracted from the base image. Both the base image and enhancement image are dispatched. Then the BTC technique is performed on the received base image, and it is decrypted by XOR and a PRND to give the reconstructed base output. The Full original Image is reconstructed by adding the enhancement image to the base image, and then it is decrypted by XOR and a PRND to give the full rebuilt output.

3.1. Image Encoding

3.1.1. Image Encryption

The input grey image has a pixel value in the range of 0 to 255. It has a matrix size of L1×L2. The PRND is generated, and its value falls between 0 and 255 of size L1×L2. Then the XOR operation is taken with the input grey image and a PRND. The encrypted Image $Le(m,n)$ is given by Equation (1) as

$$Le(m,n) = xor(L(m,n), rnd(m,n)) \quad (1)$$

Where $L(m,n)$ is the input grey image, $rnd(m,n)$rn is the PRND generated value, m is the size of the row equal to L1, and n is the size of the column equal to L2. The PRND-generated value is supplied to the receiver side. Figure 2 and Figure 3 display the primary Image and the encrypted Image.

3.1.2. Image Compression

The encrypted Image $Le(m,n)$ is separated into NOL of size 4×4. The binary block Lb_L) is created by utilizing the mean (Lμ) as the doorstep value. The stages comprising the BTC algorithm are: -

Step 1: - The encrypted Image $Le(m,n)$ is parted into NOL of size 4×4.

Step 2: - The mean (Lμ) and variance (Lσ) are calculated for each NOL as displayed in Equations (2) and (3), where x_l is the Lth pixel value, and t denotes the aggregate number of pixels in each NOL.

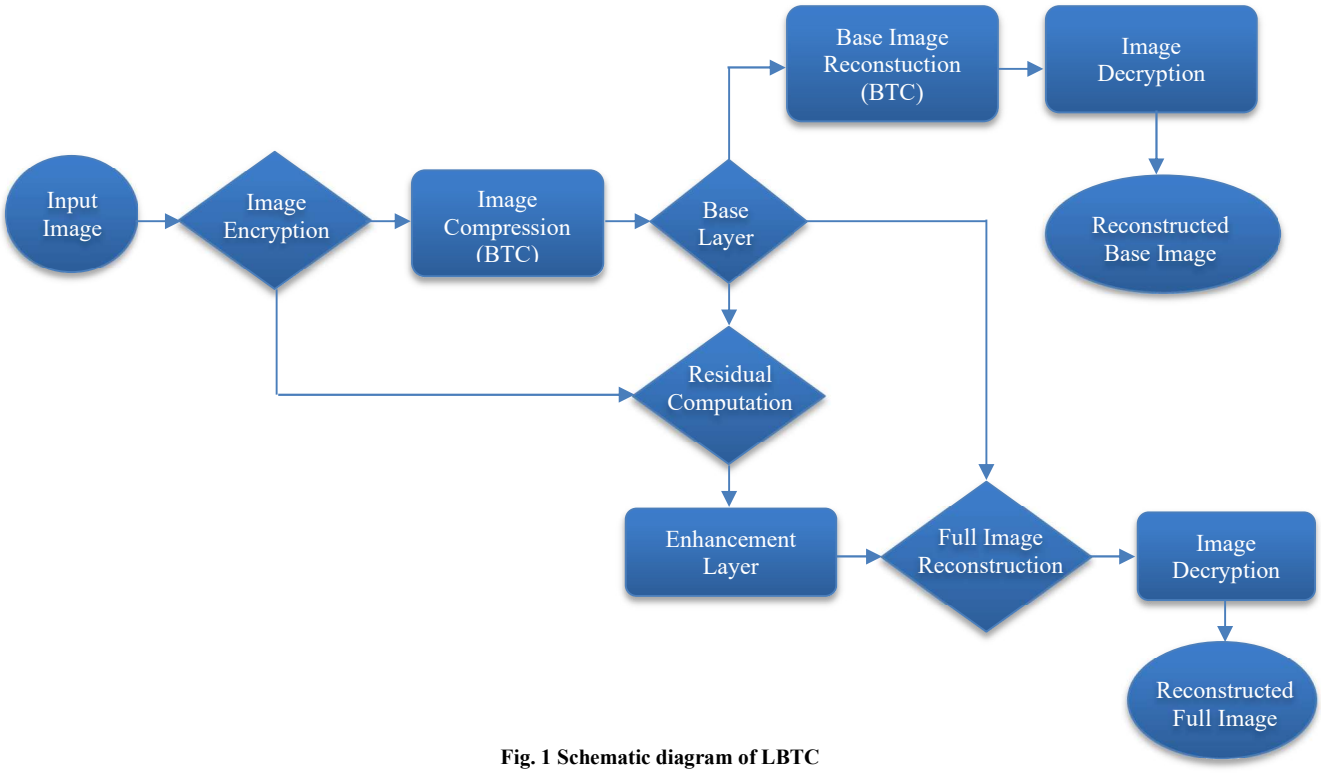

Fig. 1 Schematic diagram of LBTC

Fig. 2 Primary image

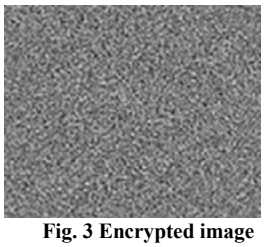

Fig. 3 Encrypted image

$$L\mu = \frac{1}{t}\sum_{L=1}^{t} x_L \tag{2}$$

$$L\sigma = \sqrt{\frac{1}{t}\sum_{L=1}^{t} (x_L - \bar{x}_L)^2} \tag{3}$$

Step 3: - The Binary Allocation matrix (Lb_L) is built by using mean (Lμ) as the doorstep value (T_L). It is given by Equation (4) as

$$Lb_L = \begin{cases} 1 & x_L \geq T_L \\ 0 & x_L < T_L \end{cases} \tag{4}$$

Where Lb_L is the L[th] intensity value of the 4×4 NOL. The binary block Lb_L It is considered the base layer of LBTC.

3.1.3. Enhancement Layer

The enhancement layer is obtained by subtracting the encrypted pixel value $Le(m,n)$ with base layer of LBTC $Lb(m,n)$. It is given by Equation (5) as

$$Len(m,n) = Le(m,n) - Lb(m,n) \tag{5}$$

It is further quantized by dividing it by the quantization step size, where the quantization step size is taken as 1, and then balanced to the nearest integer value. The smaller the quantization step size, the better the image quality. Both Base Layer $Lb(m,n)$ and Enhancement Layer $Le(m,n)$ are transmitted.

3.2. Image Decoding

3.2.1. Image Reconstruction

Base Reconstruction

The base layer content $Lb(m,n)$ *The* received signal at the receiver side is rebuilt by using the BTC technique. The Lo is the aggregate of '0's and L_H is the aggregate of '1's in the non-overlapping block of size 4×4. The equations to calculate LHI and LLO values are displayed in Equations (6) and (7).

$$\text{LHI} = L\mu + \text{L}\sigma\sqrt{\frac{L_O}{L_H}} \tag{6}$$

$$\text{LLO} = L\mu - \text{L}\sigma\sqrt{\frac{L_H}{L_O}} \tag{7}$$

Then the base image is rebuilt by replacing '0' as LLO and '1' as LHI, which is displayed in Equation (8) as:

$$LBbase(m,n) = \begin{cases} \text{LHI}, & Lb(m,n) = 1 \\ \text{LLO}, & Lb(m,n) = 0 \end{cases} \tag{8}$$

Full Reconstruction

The full primary Image is rebuilt by adding the base layer $Lb(m,n)$ with the enhancement layer content $Le(m,n)$ and the resultant content is clamped with (0,255) values. It is given by Equation (9) as,

$$Lbfull\,(m,n) = Lb(m,n) + Len(m,n) \quad (9)$$

3.2.2. Image Decryption

Base Decryption

The final original base image is rebuilt by taking an XOR operation with the base content $LBbase(m,n)$ and PRND $rnd(m,n)$. It is given by Equation (10) as

$$LBbasefinal(m,n) = xor\big(LBbase(m,n), rnd(m,n)\big) \quad (10)$$

The reconstructed base content is displayed in Figure 4.

Full Decryption

The final full original Image is rebuilt by taking the XOR operation with the full content $LBfull(m,n)$ and PRND $rnd(m,n)$. It is given by Equation (11) as

$$LBfullfinal(m,n) = xor(Lbfull(m,n), rnd(m,n)) \quad (11)$$

The reconstructed original Image (full content) is displayed in Figure 5.

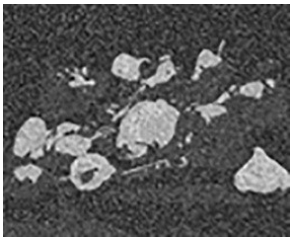

Fig. 4 Reconstructed base image

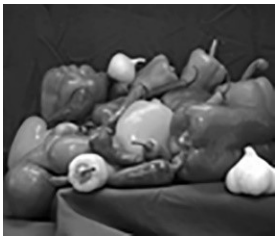

Fig. 5 Reconstructed full image

4. Experimental Findings

4.1. Correlation between Primary and Recreated Full Image

Figure 6 displays the correlation between the primary and the recreated full Image. Figure 7 reveals that the reconstructed full Image by the proposed system has superior quality, besides the functioning techniques such as BTC, Hadamard, and RDH-AMBTC.

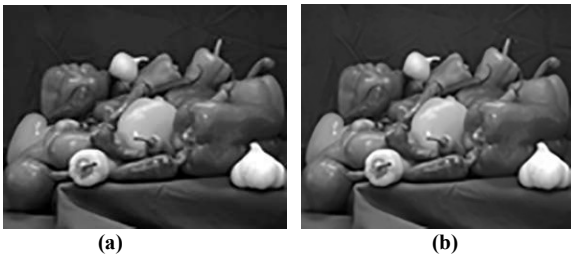

(a) **(b)**

Fig. 6 Correlation among the primary and the recreated full Image (a). primary image (b). recreated full image

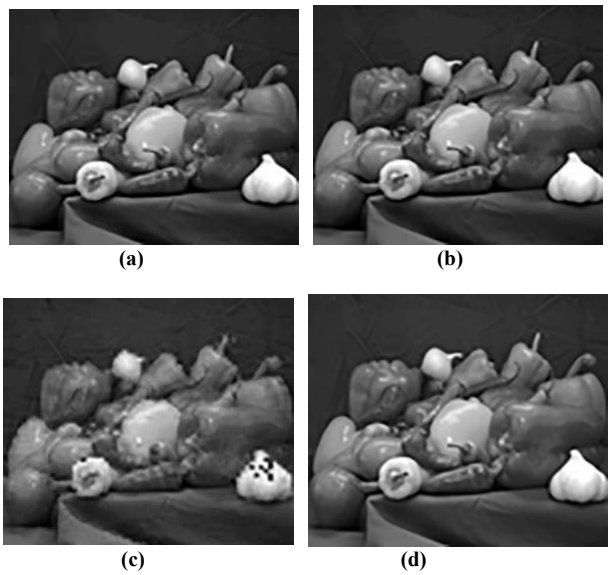

(a) **(b)** **(c)** **(d)**

Fig. 7 Correlation among LBTC with other techniques (a) RDH-AMBTC, (b) Hadamard, (c) BTC, (d) LBTC.

4.2. CR

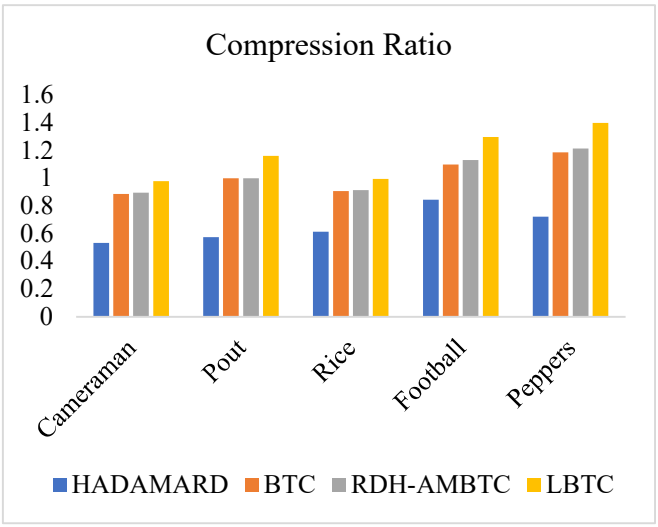

Fig. 8 CR values for techniques such as Hadamard, BTC, RDH-AMBTC, and LBTC for different Images

The CR is a parameter that represents the amount of storage reduced in size. The CR is based on the compression algorithm [17] used. The CR is acquired by dividing the non-compressed file size by the downsized file size.

The CR formula is given as:

$$CR = \frac{file\ size\ of\ the\ non-compresse\ \ image}{file\ size\ of\ downsized\ image} \quad (12)$$

The CR values for techniques such as Hadamard, BTC, RDH-AMBTC, and LBTC for diverse images are displayed in Figure 8. Figure 8 compares the CR achieved by the proposed LBTC method with RDH-AMBTC, Hadamard, and BTC.

The proposed LBTC method attained the highest CR of 1.6559 compared with 1.0307 for RDH-AMBTC, 0.6569 for Hadamard, and 1.0156 for BTC. This corresponds to improvements of approximately 13.1%, 77.48%, and 14.77%, respectively. The results indicate that the proposed LBTC method provides more efficient image compression while maintaining the desired reconstruction performance.

4.3. BR

Bit rate [17] is used to compute the number of bits throughput per unit time. The lower bit rate is preferred, which reflects that the algorithm used has superior performance. The BR formula is given as:

$$bit\ rate = \frac{m}{compression\ ratio} \tag{13}$$

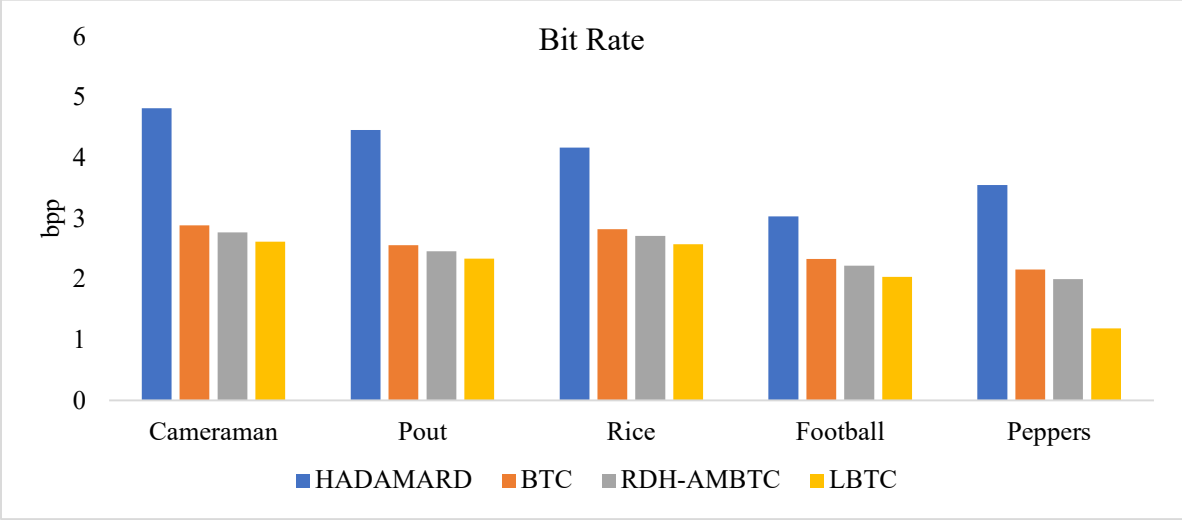

Fig. 9 BR values for techniques such as Hadamard, BTC, RDH-AMBTC, and LBTC for different Images

Where m is the cumulative bits of the non-compressed Image, the BR values for techniques such as RDH-AMBTC, Hadamard, BTC, and LBTC for diverse images are exhibited in Figure 9. Figure 9 compares the BR of the proposed LBTC with RDH-AMBTC, Hadamard, and BTC. The proposed LBTC achieved the lowest BR of 2.1488, compared with 2.4330, 4.0061 and 2.5518 for RDH-AMBTC, Hadamard, and BTC, respectively. This represents bit rate reductions of 11.68%, 46.36%, and 15.79%, respectively, indicating improved coding efficiency with fewer bits required for image representation.

4.4. MSE

The MSE [17] is a benchmark used to compute the precision of the reconstructed full Image. The MSE is evaluated in the middle of the primary Image and the reconstructed full Image. The lower MSE value reflects that the reconstructed full Image has superior image quality. The MSE is computed as:

$$MSE = \frac{1}{ij}\sum_{m=1}^{i}\sum_{n=1}^{j}[LBfullfinal(m,n) - L(m,n)]^2 \tag{14}$$

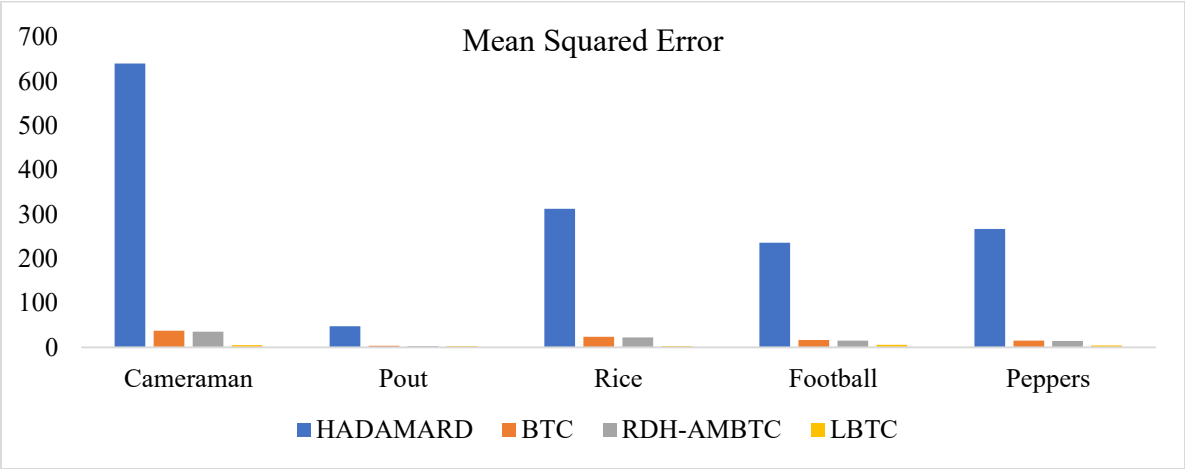

Fig. 10 MSE values for techniques such as Hadamard, BTC, RDH-AMBTC, and LBTC for different Images

Where $LBfullfinal(m,n)$ stands for downsized Image, $L(m,n)$ stands for the primary Image, and j and I typify the dimensions of columns and rows in both images, respectively.

The MSE values for techniques such as BTC, Hadamard, RDH-AMBTC, and LBTC for diverse images are presented in Figure 10. Figure 10 compares the MSE of the proposed LBTC with RDH-AMBTC, Hadamard, and BTC.

The proposed LBTC achieved the lowest MSE of 4.2200, compared with 18.0789, 300.9356, and 19.2481 for RDH-AMBTC, Hadamard, and BTC, respectively. This corresponds to MSE reductions of 76.66%, 98.60%, and 78.08%, respectively, indicating that the proposed method reconstructs images with substantially lower error than the existing techniques.

4.5. wMSE

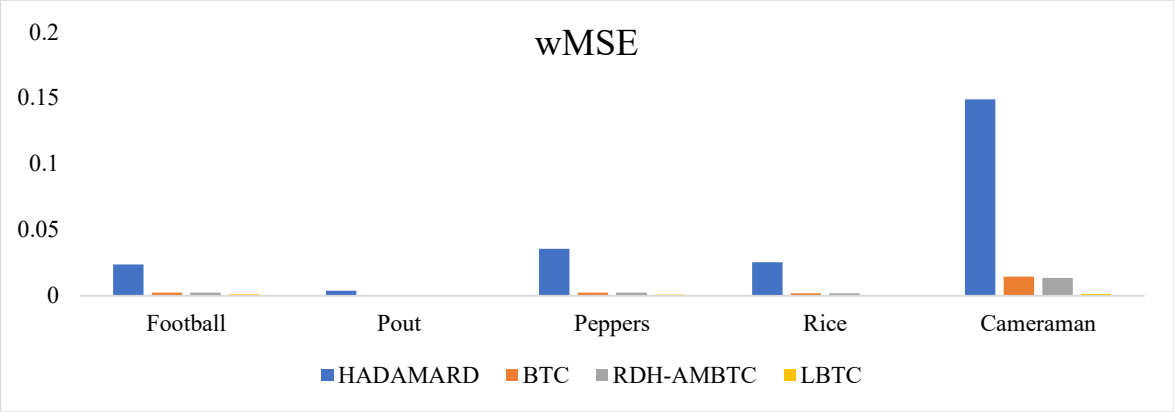

Fig. 11 wMSE values for techniques such as Hadamard, BTC, RDH-AMBTC, and LBTC for different images

The wMSE [17] is also a benchmark used to compute the precision of the reconstructed full Image. The wMSE is measured by the sum of squared differences in the middle of the primary Image and the reconstructed full Image. The smaller the wMSE value, the better the reconstructed full Image has superior image quality. The wMSE formula is given as:

$$wMSE = \frac{1}{ij}\sum_{m=1}^{i}\sum_{n=1}^{j}\left(2\left|\frac{LBfullfinal(m,n)-L(m,n)}{LBfullfinal(m,n)+L(m,n)}\right|\right)^2 \quad (15)$$

Where $LBfullfinal(m,n)$ stands for the downsized Image, $L(m,n)$ stands for the primary Image, and I and I typify the dimensions of columns and rows in both images, respectively.

The wMSE values for techniques such as BTC, Hadamard, RDH-AMBTC, and LBTC for diverse images are exposed in Figure 11. Figure 11 compares the wMSE of the proposed LBTC with RDH-AMBTC, Hadamard, and BTC. The proposed LBTC achieved the lowest MSE of 0.00078, compared with 0.00396, 0.04748, and 0.0042 for RDH-AMBTC, Hadamard, and BTC, respectively. This corresponds to wMSE reductions of 80.30%, 98.36%, and 81.43%, respectively, indicating improved reconstruction accuracy with substantially lower weighted error than the existing methods.

4.6. PSNR

The PSNR [17, 23, 24] measures the degradation level of the reconstructed full Image. The greater the PSNR value, the more it reflects that the reconstructed full Image has superior image quality. The PSNR formula is given as:

$$PSNR = 10\,log_{10}\frac{255^2}{MSE} \quad (16)$$

Where MSE stands for mean squared error.

The PSNR of techniques such as Hadamard, BTC, RDH-AMBTC, and LBTC for diverse images is exhibited in Figure 12. Figure 12 compares the PSNR of the proposed LBTC with RDH-AMBTC, Hadamard, and BTC. The proposed LBTC achieved the highest PSNR of 42.0910 dB, compared with 33.8484 dB, 24.5707 dB, and 24.5709 dB for RDH-AMBTC, Hadamard, and BTC, respectively. This corresponds to PSNR improvements of 24.35%, 71.30%, and 71.29%, respectively, indicating that the proposed method provides the highest reconstructed image quality with lower distortion.

4.7. wPSNR

The wPSNR [17] is an advanced version of PSNR and gives an accurate estimate of the degradation level of the reconstructed full Image. The greater the wPSNR value, the more it reflects that the reconstructed full Image has superior image quality. The wPSNR formula is given as:

$$wPSNR = 10\,\log_{10}\left(\frac{255^2}{wMSE}\right) \quad (17)$$

Where wMSE stands for weighted mean squared error.

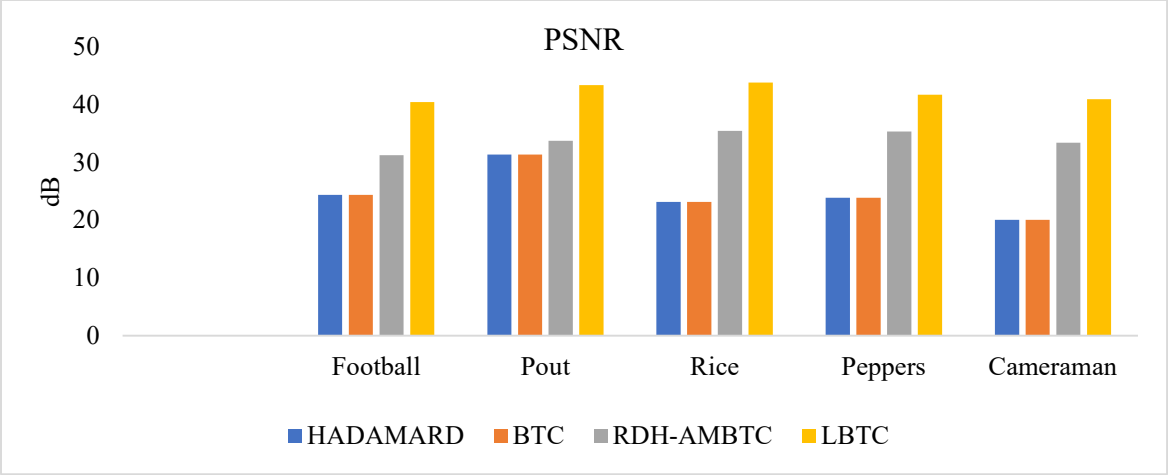

Fig. 12 PSNR values for techniques such as Hadamard, BTC, RDH-AMBTC, and LBTC for different images

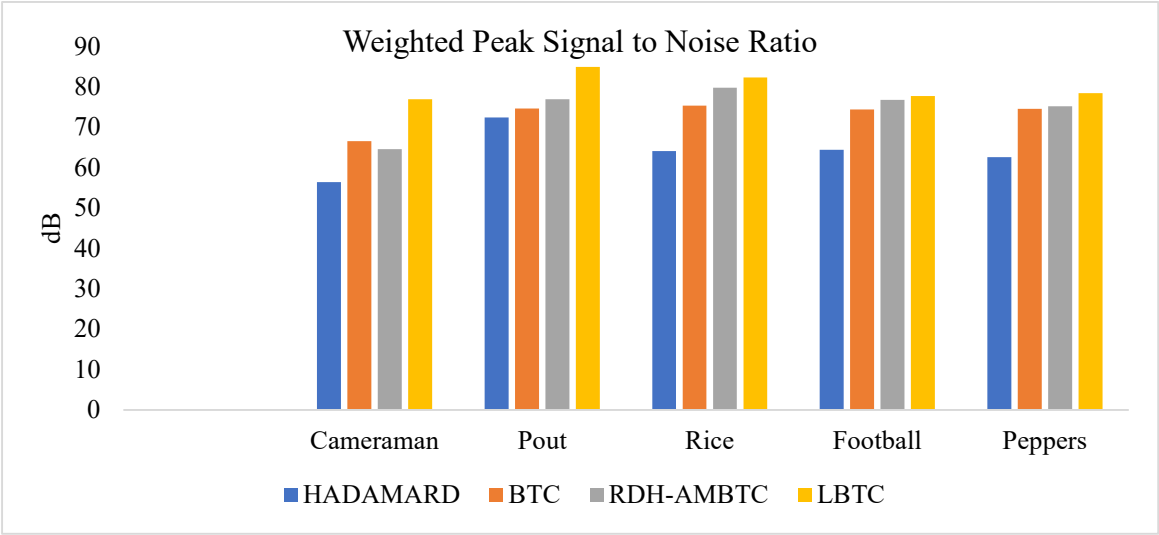

Fig. 13 wPSNR values for techniques such as RDH-AMBTC, Hadamard, BTC, and LBTC for different images

The wPSNR is matched up among approaches, such as Hadamard, BTC, RDH-AMBTC, and LBTC, for diverse images as shown in Figure 13.

Figure 13 compares the wPSNR of the proposed LBTC with RDH-AMBTC, Hadamard, and BTC. The proposed LBTC achieved the highest wPSNR of 80.0897 dB compared with 74.6684 dB, 63.9799 dB, and 73.1295 dB for RDH-AMBTC, Hadamard, and BTC, respectively. This corresponds to wPSNR improvements of 7.26 %, 25.18%, and 9.52%, respectively, indicating enhanced weighted reconstruction quality with reduced perceptual distortion.

4.8. Computational Time

The computational time required for approaches such as Hadamard, BTC, RDH-AMBTC, and LBTC for different images is displayed in Figure 14.

Figure 14 compares the computational time of the proposed LBTC with RDH-AMBTC, Hadamard, and BTC. The proposed LBTC achieved the lowest computational time of 2.8854 ms compared with 26.5589 ms, 22.0130 ms, and 12.0422 ms for RDH-AMBTC, Hadamard, and BTC, respectively. This corresponds to computational time reductions of 89.14%, 86.89%, and 76.04%, respectively, demonstrating the computational efficiency of the proposed method.

The System Configuration used is:

S/w:-
Matlab R2016a and Windows 10
H/w:-
System: 64-bit o/s
RAM 4.00 GB
Processor: Intel i3 CPU 1.70 GHz

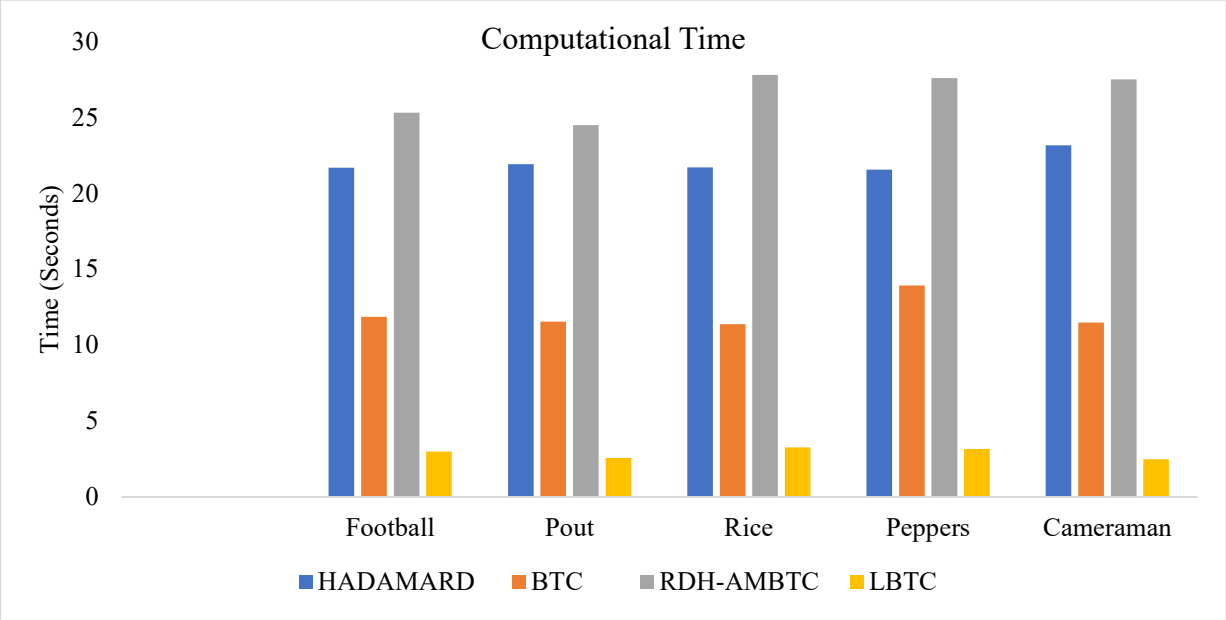

Fig. 14 Computational time required for approaches such as Hadamard, BTC, RDH-AMBTC, and LBTC for different images.

4.9. Memory Size

The memory size required for techniques such as Hadamard, BTC, RDH-AMBTC, and LBTC for different images is displayed in Figure 15. Figure 15 compares the memory usage of the proposed LBTC with RDH-AMBTC, Hadamard, and BTC. The proposed LBTC required the lowest memory size of 1325.4 MB compared with 1447.8 MB, 1698.2 MB, and 1732.8MB for RDH-AMBTC, Hadamard, and BTC, respectively. This corresponds to memory usage reductions of 8.45%, 21.95%, and 23.51%, respectively, demonstrating the memory efficiency of the proposed method.

Figure 16 correlates the diverse State-of-the-Art (s-o-t) techniques [20-25, 28-30] with the LBTC. The test image employed is the pepper image, and the parameter employed is PSNR. The plot displays that the proposed system, LBTC, is far superior to functioning s-o-t techniques. This is made possible due to the novelty of the proposed LBTC technique by using a base layer and an enhancement layer to rebuild the principal content closer to the primary Image, which leads to a higher PSNR (41.73 dB than existing techniques. The images used for performance analysis are shown in Figures 17(a)-(e).

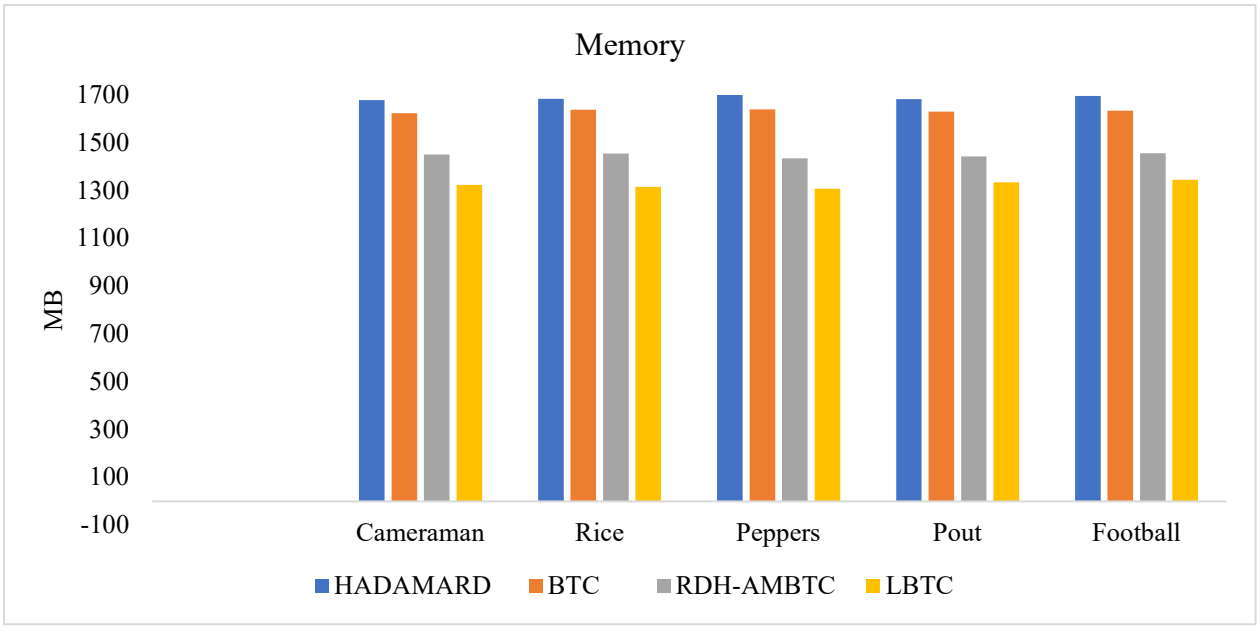

Fig. 15 Memory size required for techniques such as Hadamard, BTC, RDH-AMBTC, and LBTC for different images

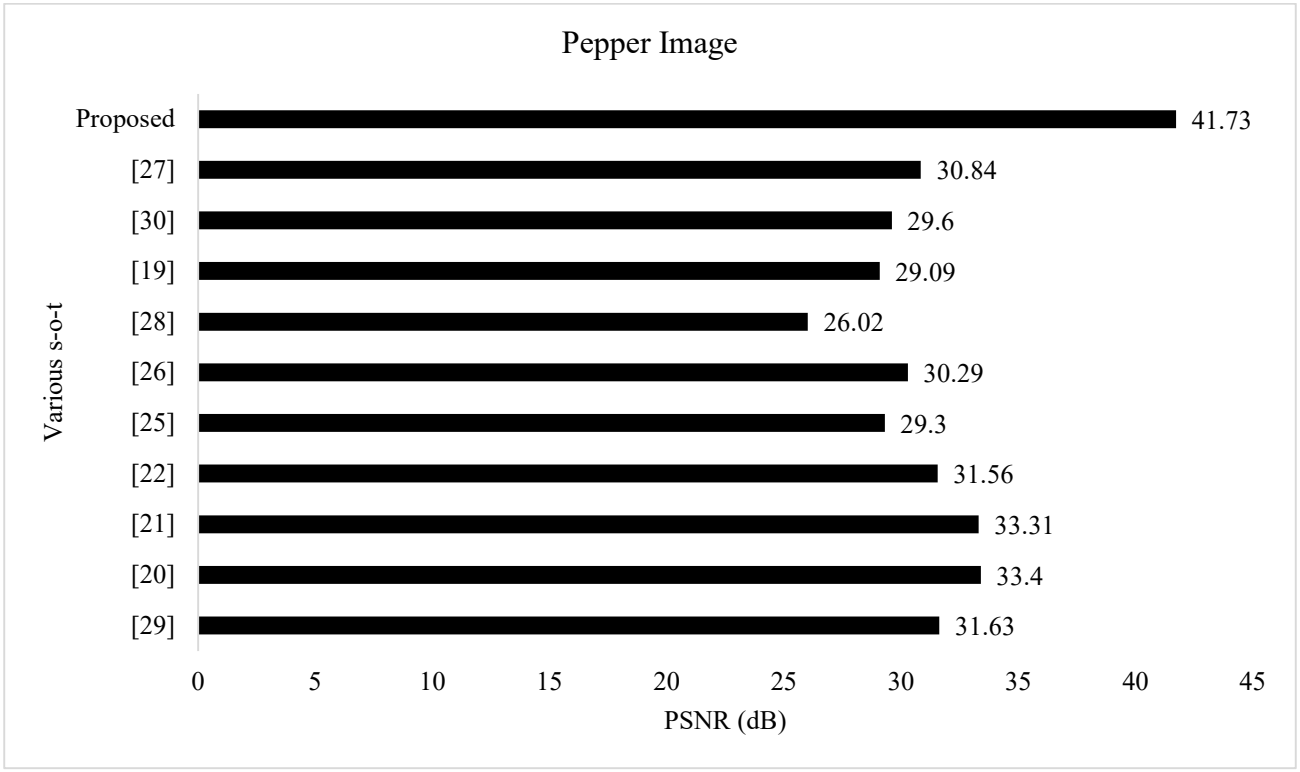

Fig. 16 Correlation between various s-o-t techniques with the proposed LBTC

Fig. 17(a) Pout

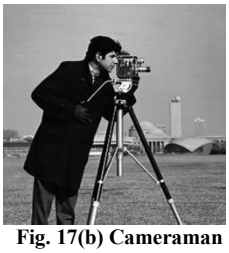

Fig. 17(b) Cameraman

Fig. 17(c) Rice

Fig. 17(d) Peppers

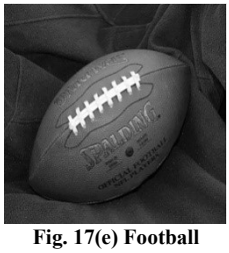

Fig. 17(e) Football

5. Conclusion

The novel method of SCE images using LBTC is proposed. The input grey image is encrypted using PRND and XOR operation, then the base image is obtained by performing the BTC technique, and also the base image is subtracted from the encrypted Image to get the enhancement image. Both the Base image and the enhancement image are dispatched. At the receiver side, the enhanced Image is added with the base image and then decrypted by using the XOR operation and PRND to get the rebuilt full original Image. The base image is rebuilt using the BTC technique and then decrypted by using the XOR operation and PRND to get the rebuilt base original Image. The proposed LBTC technique is far superior to functioning techniques such as RDH-AMBTC, Hadamard, and BTC in relation to CR, computing time, memory size, PSNR, MSE, wPSNR, wMSE, and BR. Thus, it develops the proposed system more suitable for any image processing applications in terms of secure transmission and reduced storage space requirements.

Competing Interests

There are no competing interests regarding the subject matter/core part of the research being proposed through this paper, and there are no direct/indirect financial involvements or competing interests in relevance throughout the articulation/preparation of this research paper.

References

[1] Wentao Ma et al., "A Privacy-Preserving Content-based Image Retrieval Method based on Deep Learning in Cloud Computing," *Expert Systems with Applications*, vol. 203, pp. 1-12, 2022. [CrossRef] [Google Scholar] [Publisher Link]

[2] Markovskyi Oleksandr et al., "Method of Protecting Data Processed by the Discrete Fourier Transform in Remote Computer Systems," *2022 12th International Conference on Dependable Systems, Services and Technologies (DESSERT)*, Athens, Greece, pp. 1-5, 2022. [CrossRef] [Google Scholar] [Publisher Link]

[3] Ying Sun et al., "Secure Filtering under Adaptive Event-triggering Protocols with Memory Mechanisms," *ISA Transactions*, vol. 127, pp. 13-21 2022. [CrossRef] [Google Scholar] [Publisher Link]

[4] Tiziano Bianchi, Alessandro Piva, and Mauro Barni, "Composite Signal Representation for Fast and Storage-Efficient Processing of Encrypted Signals," *IEEE Transformation on Information Forensics and Security*, vol. 5, no. 1, pp. 180-187, 2010. [CrossRef] [Google Scholar] [Publisher Link]

[5] Ashwani Kumar, "A Cloud-based Buyer-seller Watermarking Protocol (CB-BSWP) using Semi-trusted Third Party for Copy Deterrence and Privacy Preserving," *Multimedia Tools and Applications*, vol. 81, pp. 21417-21448, 2022. [CrossRef] [Google Scholar] [Publisher Link]

[6] Jenny Heino et al., "On Usability of Hash Fingerprinting for Endpoint Application Identification," *2022 IEEE International Conference on Cyber Security and Resilience (CSR)*, Rhodes, Greece, pp. 38-43, 2022. [CrossRef] [Google Scholar] [Publisher Link]

[7] M. Johnson et al., "On Compressing Encrypted Data," *IEEE Transactions on Signal Processing*, vol. 52, no. 10, pp. 2992-3006, 2004. [CrossRef] [Google Scholar] [Publisher Link]

[8] Daniel Schonberg, Stark C. Draper, and Kannan Ramchandran, "On Blind Compression of Encrypted Correlated Data Approaching the Source Entropy Rate," *2005 13th European Signal Processing Conference*, Allerton, IL, USA, pp. 1-4, 2005. [Google Scholar] [Publisher Link]

[9] Riccardo Lazzeretti, and Mauro Barni, "Lossless Compression of Encrypted Grey Level and Color Images," *2008 16th European Signal Processing Conference, Lausanne, Switzerland*, Lausanne, Switzerland, pp. 1-5, 2008. [Google Scholar] [Publisher Link]

[10] Xilin Liu, Andrew G. Richardson, and Jan Van der Spiegel, "An Energy-Efficient Compressed Sensing-Based Encryption Scheme for Wireless Neural Recording," *IEEE Journal on Emerging and Selected Topics in Circuits and Systems*, vol. 11, no. 2, pp. 405-414, 2021. [CrossRef] [Google Scholar] [Publisher Link]

[11] Xinpeng Zhang, "Lossy Compression and Iterative Reconstruction for Encrypted Image," *IEEE Transactions on Information Forensics and Security*, vol. 6, no. 1, pp. 53-58, 2011. [CrossRef] [Google Scholar] [Publisher Link]

[12] A. Bilgin et al., "Scalable Image Coding using Reversible Integer Wavelet Transforms," *IEEE Transactions on Image Processing*, vol. 9, no. 11, pp. 1972-1977, 2000. [CrossRef] [Google Scholar] [Publisher Link]

[13] D. Taubman, "High Performance Scalable Image Compression with EBCOT," *IEEE Transactions on Image Processing*, vol. 9, no. 7, pp. 1158-1170, 2000. [CrossRef] [Google Scholar] [Publisher Link]

[14] Xinpeng Zhang et al., "Scalable Coding of Encrypted Images," *IEEE Transactions on Image Processing*, vol. 21, no. 6, pp. 3108-3114, 2012. [CrossRef] [Google Scholar] [Publisher Link]

[15] E. Delp, and O. Mitchell, "Image Compression Using Block Truncation Coding," *IEEE Transactions on Communications*, vol. 27, no. 9, pp. 1335-1342, 1979. [CrossRef] [Google Scholar] [Publisher Link]

[16] M. Lema, and O. Mitchell, "Absolute Moment Block Truncation Coding and Its Application to Color Images," *IEEE Transactions on Communications*, vol. 32, no. 10, pp. 1148-1157, 1984. [CrossRef] [Google Scholar] [Publisher Link]

[17] P. Jeya Bright, and G. Vishnuvarthanan, "Development of a Scalable Coding for the Encryption of Images using Block Truncation Code," *2019 3rd International Conference on Trends in Electronics and Informatics (ICOEI)*, Tirunelveli, India, pp. 934-938, 2019. [CrossRef] [Google Scholar] [Publisher Link]

[18] Cheonshik Kim, "Separable Reversible Data Hiding in Encrypted AMBTC Images Using Hamming Code," *Applied Sciences*, vol. 12, no. 16, pp. 1-16, 2022. [CrossRef] [Google Scholar] [Publisher Link]

[19] Ching-Nung Yang et al., "Constructions of General (*k,n*) Reversible AMBTC-based Visual Cryptography with Two Decryption Options," *Journal of Visual Communication and Image Representation*, vol. 48, pp. 182-194, 2017. [CrossRef] [Google Scholar] [Publisher Link]

[20] Guo-Dong Su, Chin-Chen Chang, and Chia-Chen Lin, "A High Capacity Reversible Data Hiding in Encrypted AMBTC-Compressed Images," *IEEE Access*, vol. 8, pp. 26984-27000, 2020. [CrossRef] [Google Scholar] [Publisher Link]

[21] Chih-Cheng Chen et al., "TSIA: A Novel Image Authentication Scheme for AMBTC-Based Compressed Images Using Turtle Shell Based Reference Matrix," *IEEE Access*, vol. 7, pp. 149515-149526, 2019. [CrossRef] [Google Scholar] [Publisher Link]

[22] Zhan Yu et al., "HBF-DH: An Enhanced Payload Hybrid Data Hiding Method Based on a Hybrid Strategy and Block Features," *IEEE Access*, vol. 7, pp. 148439-148452, 2019. [CrossRef] [Google Scholar] [Publisher Link]

[23] Stephen Welstead, *Fractal and Wavelet Image Compression Techniques*, SPIE Publication, vol. TT40, pp. 1-254, 1999. [CrossRef] [Google Scholar] [Publisher Link]

[24] Raouf Hamzaoui, Dietmar Saupe, and M. Barni, *Fractal Image Compression*, Document and Image Compression, CRC Press, 2006. [Google Scholar] [Publisher Link]

[25] J.C. Chuang, and C.C. Chang, "Using a Simple and Fast Image Compression Algorithm to Hide Secret Information," *International Journal of Computers and Applications*, vol. 28, no. 4, pp. 329-333, 2006. [CrossRef] [Google Scholar] [Publisher Link]

[26] Duanhao Ou, and Wei Sun, "High Payload Image Steganography with Minimum Distortion based on Absolute Moment Block Truncation Coding," *Multimedia Tools and Applications*, vol. 74, pp. 9117-9139, 2014. [CrossRef] [Google Scholar] [Publisher Link]

[27] Aruna Malik, Geeta Sikka, and Harsh K. Verma, "A High Payload Data Hiding Scheme based on Modified AMBTC Technique," *Multimedia Tools and Applications*, vol. 76, pp. 14151-14167, 2017. [CrossRef] [Google Scholar] [Publisher Link]

[28] Jiantao Zhou et al., "Scalable Compression of Stream Cipher Encrypted Images through Context-Adaptive Sampling," *IEEE Transactions on Information Forensics and Security*, vol. 9, no. 11, pp. 1857-1868, 2014. [CrossRef] [Google Scholar] [Publisher Link]

[29] Chia-Chen Lin et al., "A Novel Reversible Data Hiding Scheme Based on AMBTC Compression Technique," *Multimedia Tools and Applications*, vol. 74, pp. 3823-3842, 2013. [CrossRef] [Google Scholar] [Publisher Link]

[30] Chia-Chen Lin, Juan Lin, and Chin-Chen Chang, "Reversible Data Hiding for AMBTC Compressed Images Based on Matrix and Hamming Coding," *Electronics*, vol. 10, no. 3, pp. 1-20, 2021. [CrossRef] [Google Scholar] [Publisher Link]